The Role of Retained Austenite Stability on Low-Temperature Mechanical Behaviors of a Quenching and Partitioning Steel

Z. WANG and M.X. HUANG

Low-temperature deformation and fracture behaviors are studied for a quenching and partitioning (Q&P) steel by interrupted tensile tests and X-ray diffraction (XRD). The austenite stability decreases significantly from 298 K to 223 K, while further cooling to 77 K does not cause greater instability. The yielding, work hardening, and fracture behaviors are found to change under the influence of austenite stability at low temperatures.

https://doi.org/10.1007/s11661-019-05465-w

I. INTRODUCTION

MANY advanced high-strength steels (AHSS) have been newly developed for lightweight automotive applications.[1–6] Despite the excellent balance of strength and ductility, the unsatisfactory in-use properties keep these new automotive steels from practical applications.[1–3,7] Among various in-use properties, low-temperature mechanical behaviors are essential to ensure the safety of automotive steels. As temperature decreases, it becomes more difficult for dislocations to move inside the microstructure, which can induce undesired brittle fracture.[8,9] The phenomenon is called cold brittleness. In many cities around the world, winter temperatures can be much lower than 0 °C, the temperature where cold brittleness is commonly observed in steels. Therefore, to promote their industrial applications, AHSS should be designed carefully to make sure that the mechanical properties do not degrade too much at low temperatures.

Quenching and partitioning (Q&P) steels belong to the third generation of AHSS, containing a multiphase microstructure of martensite matrix (sometimes partially ferrite and bainite) and 10 to 20 pct retained austenite.[4–7,10] Due to the susceptibility of martensite matrix to cold brittleness, the low-temperature mechanical behaviors of Q&P steels should be studied carefully for practical applications. Besides, the behaviors of retained austenite may change significantly along with the in-use temperature.[11–14] Research shows that low temperature may reduce the stability of retained austenite and promote deformation-induced martensite transformation (DIMT),[14] which influences the yield strength, work hardening, fracture behaviors, and other mechanical properties.[11–13] When the retained austenite stability decreases, the risk of brittle fracture is also likely to increase.[15] In a word, the low-temperature deformation and fracture of Q&P steels can be even more complicated due to the presence of the metastable phase. Despite the potential risks and complicated mechanisms, studies on low-temperature behaviors of Q&P steels are still very limited.

In the present work, the role of retained austenite stability on low-temperature mechanical properties is studied for a Q&P steel. Retained austenite stability was measured by X-ray diffraction (XRD), based on which the evolutions of yield strength, work hardening, and fracture behaviors at low temperatures are analyzed. The purpose of the present work is to draw attention to the low-temperature embrittlement risks of Q&P steels, based on which further work could be conducted to promote their industrial applications.

II. EXPERIMENTAL PROCEDURE

The chemical composition of the studied Q&P steel is Fe-0.3C-3.0Mn-1.5Si (in wt pct). For standard and interrupted tensile tests, ASTM subsize specimens with a gage length of 25 mm and a thickness of 1.2 mm were prepared along rolling direction by wire-cutting. Four test temperatures are selected in our study, 298 K, 273 K, 223 K, and 77 K (equivalent to 25 °C, 0 °C, − 50 °C, − 196 °C, respectively). The 298 K tests were carried out at ambient environment, while low-temperature specimens were firstly immerged in liquid nitrogen for at least ten minutes, and then clamped on an MTS

Z. WANG and M.X. HUANG are with the Department of Mechanical Engineering, The University of Hong Kong, Pokfulam Road, Hong Kong, China and also with the Shenzhen Institute of Research and Innovation, The University of Hong Kong, Shenzhen 518000, China. Contact e-mail: mxhuang@hku.hk
Manuscript submitted June 14, 2019.
Article published online September 30, 2019

810 Material Test System. The temperature was monitored by a thermocouple welded on the central part of tensile specimens. Tensile tests started immediately when the temperature reached the desired temperature. The crosshead displacement speed was 0.6 mm/s, corresponding to a strain rate of around 2×10^{-2} s^{-1}, so that the test finished within 10 seconds. For tests at 77 K, the specimens were wrapped by cotton soaked with liquid nitrogen to make sure that the temperature did not increase before testing. Due to the relatively high deformation rate, it is reasonable to assume the temperature at yielding the same as the starting temperature. Meanwhile, the temperature variance during deformation is not considered to affect the general trend of retained austenite stability in this study.

The volume fractions of retained austenite (V_γ) were measured with a Rigaku Smartlab X-ray diffractometer using Cu-Kα radiation. V_γ was calculated from the integrated intensities of $(110)_\alpha$, $(200)_\alpha$, $(211)_\alpha$ and $(200)_\gamma$, $(220)_\gamma$, $(311)_\gamma$ reflections. All XRD specimens were grinded and electro-polished to remove the deformed layer, and the integrated intensities were calculated through the PDXL software. Note that all XRD measurements of specimens deformed at different temperatures were conducted after the temperatures went back to room temperature. The microstructure and the electron backscattered diffraction (EBSD) characterizations were performed in LEO 1530 FEG-SEM. The fracture surface characterization was performed in Hitachi S-3400N SEM. The EBSD data were processed by HKL Channel 5 software. Specimens were electro-polished for EBSD experiments, and then etched for SEM microstructure observation. For the observation of fracture surface, specimens were ultrasonically cleaned in acetone for several minutes.

III. RESULTS AND DISCUSSION

A. *Microstructure*

The microstructure of the Q&P steel consists mainly of martensite and retained austenite, as shown in Figure 1. Considering the high alloying content, the formation of bainite is negligible during the Q&P treatment.[16] Thus, for the convenience of elaboration, the matrix is simply denoted as martensite. The retained austenite fraction is around 20 pct from EBSD analysis, while 25 pct from XRD analysis. The difference may be caused by analyzed area, detection depth, texture, and austenite distribution and grain size.[17–19] Compared with other Q&P steels, the relatively high austenite fraction here can be related to the high alloying content.[15,16,20] In addition, the retained austenite presents both filmy and bulky morphologies in this steel. According to literature, retained austenite with different morphologies is usually with different stability, which could thus lead to a continuous transformation-induced plasticity (TRIP) effect at room temperature. The continuous TRIP effect is desirable for the combination of high strength and good ductility. However, the low temperature is possible to change the austenite stability significantly into an undesirable one, which will be discussed later. Meanwhile, the grain size of coarse bulky retained austenite approaches several microns. Despite their contribution to the TRIP effect,[12] metastable retained austenite, especially the coarse bulky ones, can be detrimental to the toughness of Q&P steels.[15,20] Meanwhile, in the present steel, most martensite packet boundaries and prior austenite grain boundaries are decorated with retained austenite, which may further increase its susceptibility to intergranular fracture.[15]

B. *Retained Austenite Stability*

The stability of retained austenite at different temperatures is shown in Figure 2. Firstly, the retained austenite presents good thermal stability. As presented in Figure 2(a), the retained austenite is stable at 77 K even under elastic loading up to around 600 MPa, which can be related to the high carbon and manganese content in the steel.[16] Due to the good thermal stability, the starting microstructure before tensile testing should be the same at all the four temperatures.

The evolutions of retained austenite fraction during deformation are given in Figure 2(b). An inverse relationship is employed to describe the mechanical stability of retained austenite during tensile deformation[18]:

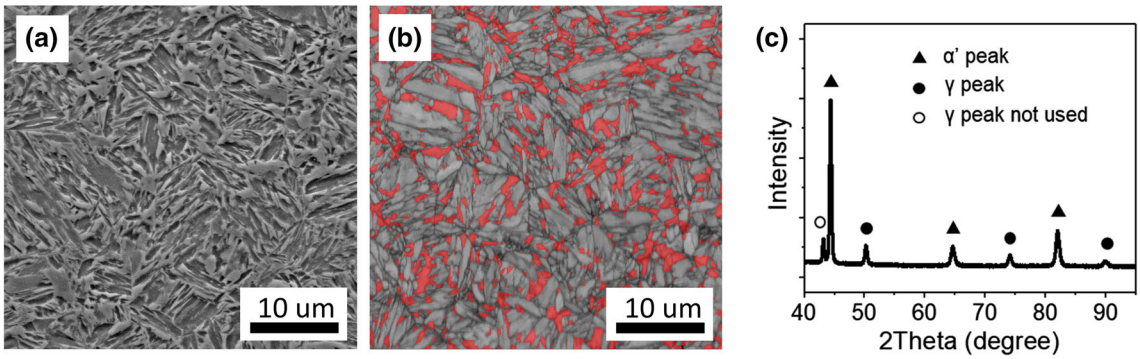

Fig. 1—Microstructure of the Q&P steel. (*a*) SEM. (*b*) EBSD (band contrast overlapped with phase map, red indicating retained austenite). (*c*) XRD. Note the first γ gamma peak is not included in the calculation of austenite fraction due to the difficulty of peak deconvolution (Color figure online).

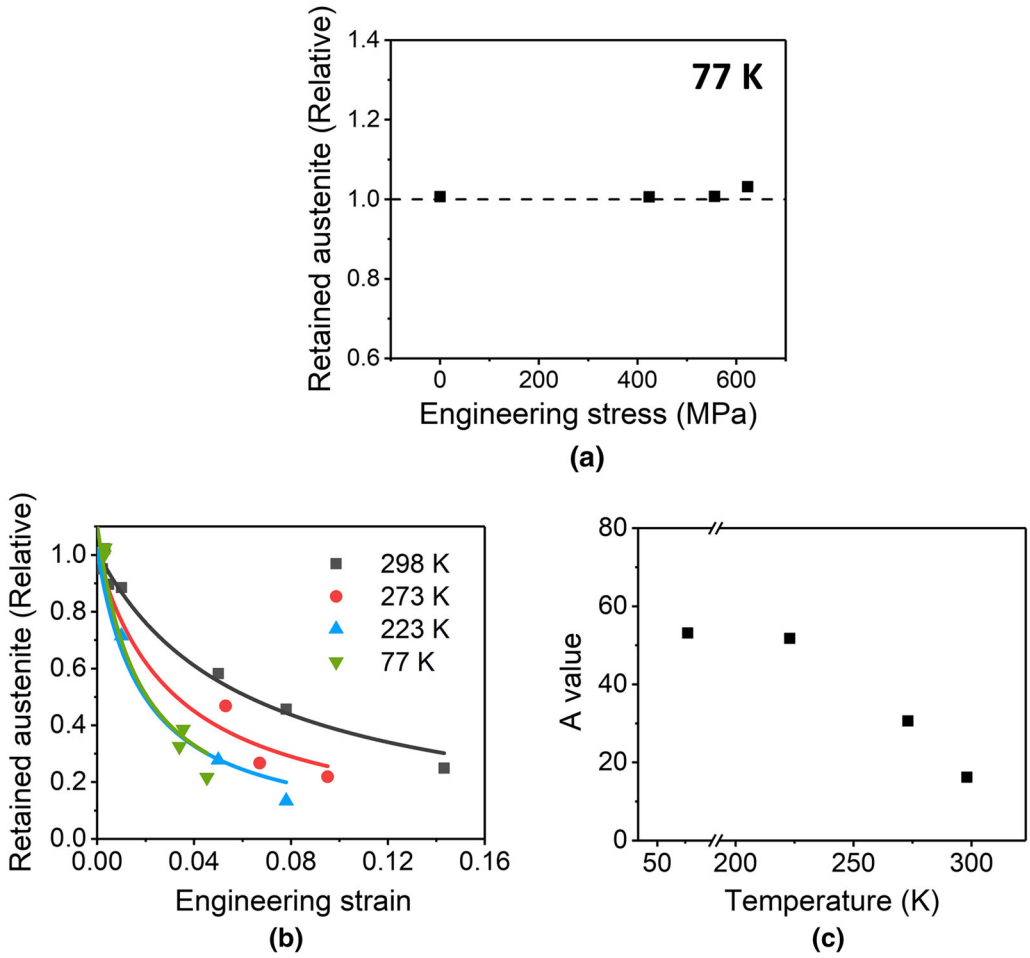

Fig. 2—Stability of retained austenite at different temperatures. (*a*) Retained austenite stability under elastic loading at 77 K. (*b*) Evolution of retained austenite volume fracture as a function of engineering strain. (*c*) A value at different test temperatures. The dashed line in (a) gives the retained austenite fraction without liquid nitrogen treatment nor loading. The solid lines in (b) are fitting curves, where A values are obtained and used as an indication of austenite stability.

$$V_\gamma = \frac{1}{A \times \varepsilon + B},$$

where ε is engineering strain, and A and B are parameters obtained through fitting. The values of A at 298 K, 273 K, 223 K, and 77 K are 16.2, 30.6, 51.8, and 53.1 in Figure 2(c), while the values of B are 0.988, 0.996, 0.982, and 0.902. Here, the A values are used as an indication of retained austenite stability. Thus, according to Figure 2(c), the mechanical stability of retained austenite decreases significantly as the test temperature decreases from 298 K to 223 K, while the stability at 223 K is close to that at 77 K. To explain this phenomenon, two competing mechanisms should be considered. On the one hand, the decreasing temperature can provide extra driving force for martensite transformation.[14] This accounts for the lower austenite stability and the faster DIMT at 223 K than those at 298 K. On the other hand, in addition to temperature, the yield strength of martensite matrix may also influence the stability of retained austenite.[21,22] At low temperatures, the martensite may become stronger and thus stabilize the retained austenite.[21–23] This can be caused by two mechanisms. Firstly, DIMT results in volume expansion which requires the accommodation of the surrounding matrix. Stronger martensite at low temperatures makes the accommodation and the transformation more difficult.[21] Secondly, harder martensite matrix may influence the partitioning of the stress between martensite and retained austenite, lowering the mean stress in the retained austenite.[21,22] However, considering the strength of retained austenite may also increase at lower temperatures,[11] the stress-partitioning mechanism still requires future examinations.

According to the above analysis, when temperature decreases from 298 K to 223 K, the difference of retained austenite stability is dominated by the extra martensite transformation driving force from temperature. Therefore, the retained austenite stability decreases. However, when temperature decreases from 223 K to 77 K, the increase of the strength of martensite matrix dominates, and maintains the stability of retained austenite.

C. *Yield Strength*

Mechanical properties at different temperatures are measured by uniaxial tensile tests. Typical engineering stress–strain curves are shown in Figure 3(a). At 298 K, the Q&P steel presents a good combination of tensile strength (over 1400 MPa) and ductility (over 16 pct). However, as the temperature decreases, the ductility decreases significantly, and the steel suffers from premature fracture without any post-uniform elongation. This means that the Q&P steel shows a severe sensitivity to cold brittleness, making the low-temperature study of great importance. The following analysis will start from the influence of retained austenite stability on yielding and work hardening behaviors, and then look further into fracture.

Figure 3(b) shows the evolution of yield strength with test temperatures. Firstly, different from most martensitic steels where yield strength increases with decreasing temperature,[8] the Q&P steel shows an unusual decrease of yield strength with decreasing temperature from 298 K to 223 K. Although rarely reported in retained-austenite-containing steels, the inverse temperature dependency has been considered a result of the TRIP effect in the field of metastable austenitic steels.[11] When deformation temperature decreases, the metastable austenite can become less stable, which makes the TRIP effect begin at a lower stress level. Then the corresponding TRIP strain, induced either by Greenwood–Johnson effect or Magee effect,[12] can lead to an earlier yielding phenomenon.

On the other hand, when temperature decreases further from 223 K to 77 K, yield strength increases again in the Q&P steel. In metastable austenitic steels, the increasing yield strength has been explained by the formation of fresh martensite at low temperatures before deformation.[11] However, according to Figure 2(a), martensite transformation cannot be observed even at the temperature of liquid nitrogen without deformation. In addition, note that the 273 K, 223 K, and 77 K specimens are all immerged into liquid nitrogen before tensile test. Thus, the formation of fresh martensite does not explain the increase of yield strength at 77 K, and further analysis is required. As shown in Figure 2(b), the evolution of retained austenite fraction with engineering strain is similar at 223 K and 77 K. However, it is shown in Figure 3(a) that under the same engineering strain, the engineering stress at 77 K is higher than that at 223 K during the whole plastic deformation process. From this perspective, the retained austenite is more stable at 77 K, and requires higher stress for martensite transformation. Therefore, the TRIP strain is delayed, and higher yield strength can be observed at 77 K.

D. *Work Hardening*

To understand the low-temperature deformation, work hardening behaviors are also studied, shown in Figure 4. The serrations of the 298 K curves could be caused by the Portevin–Le Chatelier (PLC) effect,[24,25] the disappearance of which may result from the lower carbon diffusion rate at low temperatures.[26] Figure 4(b) presents the work hardening rate at different temperatures. The work hardening rate increases with the decrease of temperature, especially from 298 K to 223 K, which should be related to the acceleration of DIMT.[11] Meanwhile, the work hardening rate is similar at 223 K and 77 K, corresponding well to their similar retained austenite stability and DIMT kinetics.

E. *Fracture Behaviors*

Despite the high work hardening rate at low temperatures which may suppress cold brittleness,[27] the elongation of the Q&P steel decreases significantly with the decreasing temperature (Figure 5). The elongation loss is similar at 273 K and 223 K, but larger at 77 K. The fracture surfaces are presented in Figure 6. At 298 K, the fracture morphology is mainly ductile dimples, while at 273 K, 233 K, and 77 K, it becomes mainly brittle intergranular fracture, corresponding to the sudden decrease of elongation at low temperatures. Between intergranular facets, ductile dimple fracture can be observed at 273 K and 233 K, but only transgranular fracture at 77 K. The fracture morphologies are

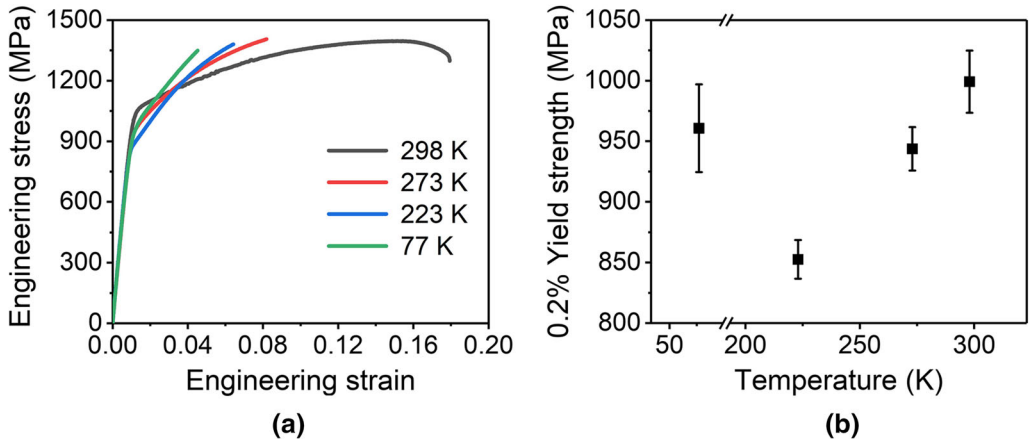

Fig. 3—(*a*) Engineering stress–strain curves and (*b*) 0.2 pct yield strength at different temperatures. The error bars give standard deviations from at least three data points.

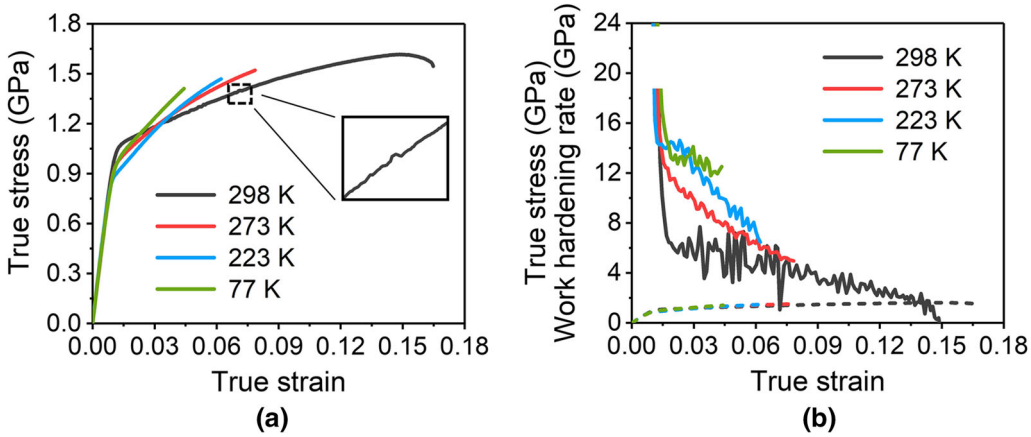

Fig. 4—(*a*) True stress–strain curves and (*b*) work hardening rates at different temperatures. The enlarged curve in (a) gives the serrations at 298 K. The dashed lines in (b) correspond to the true stress–strain curves.

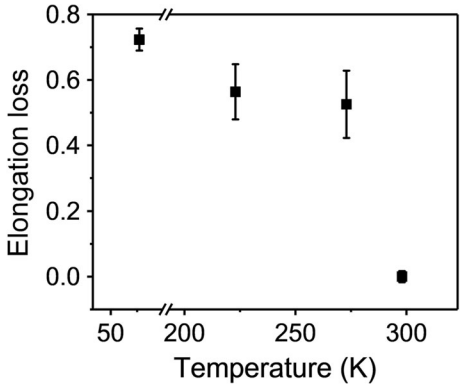

Fig. 5—Elongation loss at different temperatures. The error bars give standard deviations from at least 2 data points.

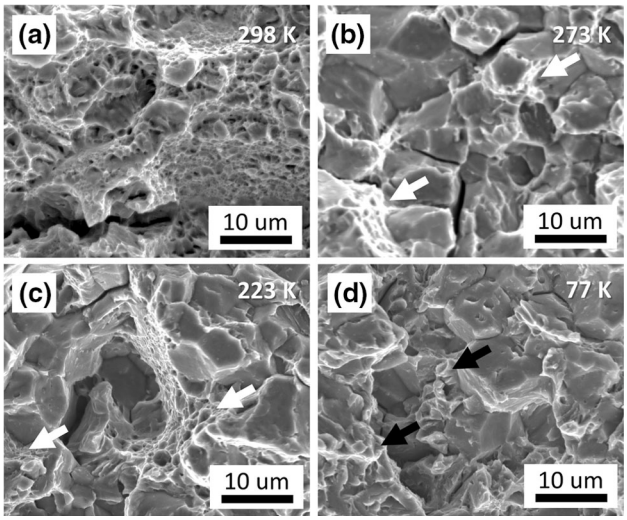

Fig. 6—Fracture surfaces at different temperatures. (*a*) 298 K. (*b*) 273 K. (*c*) 223 K. (*d*) 77 K. White arrows in (b) and (c) indicate the ductile dimple fracture between intergranular facets, while the black arrows in (d) indicate the brittle transgranular fracture.

consistent with the elongation loss in Figure 5. The fracture mechanism is discussed below.

According to the Yoffee diagram, yield stress and brittle fracture stress (either transgranular or intergranular) should be compared to analyze the fracture behaviors of martensitic steels.[8,28,29] At room temperature, as the applied stress increases, the peak stress at the crack tip reaches the yield stress first, which induces extensive plastic deformation and results in ductile fracture. On the contrary, at low temperatures, the yield stress may rise over the brittle fracture stress. Hence, the applied stress can increase to the level where the peak stress reaches the brittle fracture stress, leading to cold embrittlement. However, in the present Q&P steel, the maximum true stresses at 273 K, 223 K, and 77 K are all lower than that at 298 K, as shown in Figure 4(a), indicating that brittle fracture can be induced by even lower applied stress at low temperatures. Therefore, in addition to martensite matrix, other influential factors should also be considered.

Metastable retained austenite plays an important role in the fracture of Q&P steels and may act as brittle fracture initiators at low temperatures. As discussed above, retained austenite becomes less stable at low temperatures, and the DIMT kinetics is accordingly accelerated. DIMT can result in high carbon and untempered fresh martensite,[15] which is brittle and has proven to be the microcrack initiation location in Q&P steels.[15,20] Besides, the hard fresh martensite can cause higher micro-triaxiality and micro-stress concentration. Therefore, the faster formation of fresh martensite at low temperatures can intensify the peak stress to the brittle fracture stress and should account for the brittle fracture at even lower applied stress.

Besides, when the metastable retained austenite distributes along prior austenite grain boundaries and martensite packet boundaries (Figure 1), the accelerated DIMT tends to induce microcracks along the boundaries and lead to intergranular fracture more easily,[15] consistent with the fractographic observation in

Figure 6. Considering that the in-use environments of automotive steels are mostly above 223 K, the intergranular fracture should be of greater practical importance.

IV. CONCLUSIONS

In conclusion, the stability of retained austenite and its influence on low-temperature mechanical properties are studied for a Q&P steel. The austenite stability decreases from 298 K to 223 K, while further cooling to 77 K does not cause greater instability. The evolution of the yield strength and work hardening rate is consistent with the change of retained austenite stability at low temperatures. Finally, cold brittleness is found in the Q&P steel despite the increased work hardening rate. Reduced retained austenite stability and accelerated DIMT are responsible for the cold brittleness and the intergranular fracture morphology at low temperatures.

The present work intends to draw attention to the possible low-temperature embrittlement risks of newly developed Q&P steels. More materials and the entire in-use strain paths should be considered in the future, to provide a better understanding about the low-temperature behaviors in service.

ACKNOWLEDGMENTS

M.X. Huang acknowledges the financial support from the National Natural Science Foundation of China (No. U1764252, U1560204), Research Grants Council of Hong Kong (No. 17255016, 17203014), and National Key Research and Development Project of China (No.2017YFB0304401). The authors also acknowledge Dr. Rendong Liu and Dr. Xu Wang of Ansteel for providing the materials.

REFERENCE

1. H.L. Yi, L. Sun, and X.C. Xiong: *Mater. Sci. Technol. (UK)*, 2018, vol. 34, pp. 1112–17.
2. X. Zhu, W. Li, H. Zhao, L. Wang, and X. Jin: *Int. J. Hydrog. Energy*, 2014, vol. 39, pp. 13031–40.
3. J. Han, A.K. da Silva, D. Ponge, D. Raabe, S.M. Lee, Y.K. Lee, S.I. Lee, and B. Hwang: *Acta Mater.*, 2017, vol. 122, pp. 199–206.
4. X. Zhu, K. Zhang, W. Li, and X. Jin: *Mater. Sci. Eng. A*, 2016, vol. 658, pp. 400–08.
5. Q. Hao, S. Qin, Y. Liu, X. Zuo, N. Chen, and Y. Rong: *Mater. Sci. Eng. A*, 2016, vol. 671, pp. 135–46.
6. Y.J. Li, J. Kang, W.N. Zhang, D. Liu, X.H. Wang, G. Yuan, R.D.K. Misra, and G.D. Wang: *Mater. Sci. Eng. A*, 2018, vol. 710, pp. 181–91.
7. Z. Wang, Z.C. Luo, and M.X. Huang: *Materialia*, 2018, vol. 4, pp. 260–67.
8. K.H. Kwon, I.C. Yi, Y. Ha, K.K. Um, J.K. Choi, K. Hono, K. Oh-Ishi, and N.J. Kim: *Scr. Mater.*, 2013, vol. 69, pp. 420–23.
9. T. Sirithanakorn, M. Tanaka, and K. Higashida: *Mater. Sci. Eng. A*, 2014, vol. 611, pp. 383–87.
10. L. Wang and J.G. Speer: *Metallogr. Microstruct. Anal.*, 2013, vol. 2, pp. 268–81.
11. I. Tamura: *Met. Sci.*, 1982, vol. 16, pp. 245–53.
12. F.D. Fischer, G. Reisner, E. Werner, K. Tanaka, G. Cailletaud, and T. Antretter: *Int. J. Plast.*, 2000, vol. 16, pp. 723–48.
13. H.I. McHenry: *The Properties of Austenitic Stainless Steel At Cryogenic Temperatures*, Springer, New York, 1983.
14. S. Chatterjee and H.K.D.H. Bhadeshia: *Mater. Sci. Technol.*, 2013, vol. 23, pp. 1101–04.
15. Z. Xiong, P.J. Jacques, A. Perlade, and T. Pardoen: *Scripta Mater.*, 2018, vol. 157, pp. 6–9.
16. L. Liu, B.B. He, G.J. Cheng, H.W. Yen, and M.X. Huang: *Scripta Mater.*, 2018, vol. 150, pp. 1–6.
17. ASTM, *Standard Practice for X-Ray Determination of Retained Austenite in Steels with Near Random Crystallographic Orientation*, ASTM Standards E 975-03, 1980.
18. G.K. Tirumalasetty, M.A. Van Huis, C. Kwakernaak, J. Sietsma, W.G. Sloof, and H.W. Zandbergen: *Acta Mater.*, 2012, vol. 60, pp. 1311–21.
19. B. Verlinden, P. Bocher, E. Girault, and E. Aernoudt: *Scr. Mater.*, 2001, vol. 45, pp. 909–16.
20. M.-M. Wang, J.-C. Hell, and C.C. Tasan: *Scripta Mater.*, 2017, vol. 138, pp. 1–5.
21. X.C. Xiong, B. Chen, M.X. Huang, J.F. Wang, and L. Wang: *Scr. Mater.*, 2013, vol. 68, pp. 321–24.
22. P.J. Jacques, F. Delannay, and J. Ladrière: *Metall. Mater. Trans. A*, 2001, vol. 32A, pp. 2759–68.
23. Y. Tomita and K. Okabayashi: *Metall. Trans. A*, 1983, vol. 14, pp. 2387–93.
24. F. Yang, H. Luo, E. Pu, S. Zhang, and H. Dong: *Int. J. Plast.*, 2018, vol. 103, pp. 188–202.
25. J. Min, L.G. Hector, L. Zhang, L. Sun, J.E. Carsley, and J. Lin: *Mater. Des.*, 2016, vol. 95, pp. 370–86.
26. L.P. Kubin and Y. Estrin: *J. Phys. III*, 1991, vol. 1, pp. 929–43.
27. B. Gludovatz, A. Hohenwarter, D. Catoor, E.H. Chang, E.P. George, and R.O. Ritchie: *Science.*, 2014, vol. 345, pp. 1153–58.
28. M. Kuzmina, D. Ponge, and D. Raabe: *Acta Mater.*, 2015, vol. 86, pp. 182–92.
29. J.W. Morris, Jr: *ISIJ Int.*, 2011, vol. 51, pp. 1569–75.